Journal of Materials Chemistry A

Accepted Manuscript

This is an *Accepted Manuscript*, which has been through the Royal Society of Chemistry peer review process and has been accepted for publication.

Accepted Manuscripts are published online shortly after acceptance, before technical editing, formatting and proof reading. Using this free service, authors can make their results available to the community, in citable form, before we publish the edited article. We will replace this *Accepted Manuscript* with the edited and formatted *Advance Article* as soon as it is available.

You can find more information about *Accepted Manuscripts* in the Information for Authors.

Please note that technical editing may introduce minor changes to the text and/or graphics, which may alter content. The journal's standard Terms & Conditions and the Ethical guidelines still apply. In no event shall the Royal Society of Chemistry be held responsible for any errors or omissions in this *Accepted Manuscript* or any consequences arising from the use of any information it contains.

ROYAL SOCIETY OF CHEMISTRY

www.rsc.org/materialsA

Graphical Abstract

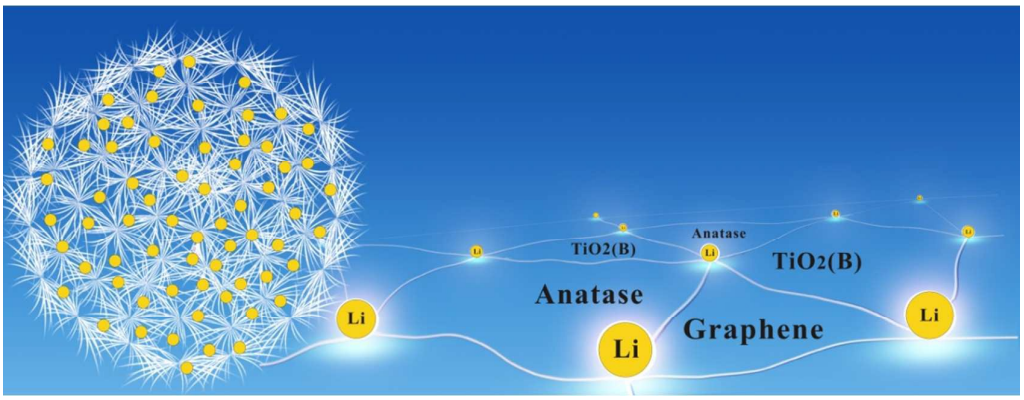

Dandelion-shape TiO_2/few layer graphene composite presents ultrahigh electrochemical properties for Li storage due to the graphene boundary-involved triphase interfacial storage mechanism.

Journal of Materials Chemistry A Accepted Manuscript

Journal Name

ARTICLE

Dandelion-shape TiO_2/Multi-layer Graphene Composed of TiO_2(B) Fibrils and Anatase TiO_2 Pappi Utilizing Triphase Boundaries for Lithium Storage

Received 00th January 20xx,
Accepted 00th January 20xx

DOI: 10.1039/x0xx00000x

www.rsc.org/

Weixin Song[a], Jun Chen[b], Xiaobo Ji[b], Xuemei Zhang[a], Fang Xie[a], D. Jason Riley[a*]

Three-dimensional dandelion-shape TiO_2/Multi-layer graphene compound (TiO_2/MLG) composed of TiO_2(B) fibrils and anatase pappi structures has been synthesized as potential anode material for Li storage. Electronmicroscopy indicates that the composite contains triphase boundaries between anatase, TiO_2(B) and graphene, which are responsible for the enhancement of energy storage and the decrease of electrode polarization. Cyclic voltammetric investigations indicate that both Li^+ insertion and pseudocapacitance contribute to charge storage. Ultrahigh specific capacities of 243 and 182 mAh g^{-1} have been obtained at 0.1 and 1 A g^{-1}, respectively. Moreover, the excellent capacity retention can reach 99.6% after 100 cycles with almost 100% coulombic efficiency at 0.1 A g^{-1}. The importance of the triphase boundary in enhancing the storage of charge and transport of Li^+ is demonstrated.

Introduction

As a consequence of an increasing demand for energy, improved energy storage is required to enable future power systems. Lithium-ion batteries offer high energy and power density and as a result are attracting great interest with a focus on designing electrodes that can enhance energy-storage performance[1, 2]. Titanium dioxide (TiO_2), one of the most promising anode materials, has been intensively studied, not only due to its low cost, abundance and non-toxicity but also on account of the negligible volume deformation during the Li-ion insertion/de-insertion processes (intercalation is preferred to describe lithium storage in a laminar host structure)[3] and excellent gravimetric capacity[3-5]. The operational potential of TiO_2 is high (>1 V *vs.* Li^+/Li), which can enhance battery safety by reducing the probability of the formation of lithium dendrites at the anode surface and avoid to form the solid electrolyte interface (SEI)[6-8]. To-date various polymorphs of TiO_2 including anatase (tetragonal)[9], rutile (tetragonal)[5], brookite (orthorhombic)[10] and bronze (TiO_2-B, monoclinic)[11]have been extensively studied as anode materials in lithium-ion batteries. The other allotropes; which either are easily transformed to other types like ramsdellite(TiO_2-R)[12] and hollandite (TiO_2-H)[13] or need high-pressure and high-temperature synthesis conditions, such as α-PbO_2-structured TiO_2(II)[14], baddeleyite[15], columbite[16], cubic[17], TiO_2(OI)[18] and TiO_2(OII)[19]; have been rarely researched. Despite the numerous studies, TiO_2 has not been used extensively as a high rate anode material owing to a limited ability to store charge and its poor conductivity.

An intrinsic drawback of TiO_2 is the material's poor electronic conductivity (10^{-13} S cm^{-1})[5, 20, 21] and limited ionic conductivity[22]. Several solutions have been proposed to overcome this issue including: (i) addition of a conducting phase, e.g., carbon coating[23] or compositing with transition metal oxides[24], (ii) reduction of the ionic diffusion length by fabricating nanoscale TiO_2 structures such as wires[25], tubes[26], cubes[27], rods[28] and flowers[8] , (iii) doping through either the introduction of Ti^{3+} or oxygen vacancies[5, 29] or with heteroatoms B[30], C[6], N[31], S[32], Ni[33], Zn[34] or Sn[35]. Charge stored in a Li^+/heterophase anode system may be enhanced [36-39] through interfacial charge storage at both the solid-liquid interface and internal solid-solid interfaces. Jamnik and Maier have demonstrated increased charge storage at TiO_2-metal interfaces as a result of the metal acting as an electron sink and the TiO_2 storing excess Li^+. In TiO_2 photochemical studies, it has been demonstrated that owing to the offset in the conduction band levels, photogenerated charge carriers can be stored at the junction between anatase and TiO_2(B)[40-42]. This band offset has been employed in TiO_2 engineering to yield a material in which Li^+ and electrons are separated across TiO_2(B)/anatase TiO_2 interfaces within the anode leading to increased charge storage.

In the present work we have fabricated a new TiO_2-graphene composite designed to enhance the prospects of this low cost,

[a] Department of Materials, Imperial College London, London SW72AZ, UK.
[b] College of Chemistry and Chemical Engineering, Central South University, Changsha 410083, China.

† Footnotes relating to the title and/or authors should appear here.
Electronic Supplementary Information (ESI) available: [details of any supplementary information available should be included here]. See DOI: 10.1039/x0xx00000x

Journal of Materials Chemistry A Accepted Manuscript

Please do not adjust margins

abundant, non-toxic material as an anode in a Li-battery. The TiO_2 is dandelion shaped with nanosized TiO_2(B) fibrils capped with anatase TiO_2 pappi. The as-prepared structure has extensive solid-electrolyte and solid-solid junctions to maximize interfacial charge storage. Multilayered graphene (MLG) is added to the TiO_2 phases to yield a composite with enhanced conductivity and an increased number of solid-solid junctions.

Experimental

Materials preparation: Dandelion-shape TiO_2/Multi-layer graphene (TiO_2/MLG) and compared TiO_2 anode materials were synthesized by solvent-thermal method. For TiO_2/MLG preparation, 0.24g polyvinylpyrrolidone (PVP, Sigma, average mole weight: 360000.) was dissolved into 40 mL acetic acid solution (Sinopharm Chemical Reagent Beijing Co. Ltd.) by strong stirring, following with the addition of 0.05g multi-layer graphene (~10nm thickness, Hefei Weijing Material Technology Co. Ltd.) and continuous stirring for 20 min. Then, 1 mL tetrabutyltitanate (TBT, Sinopharm Chemical Reagent Beijing Co. Ltd.) was added dropwise to the above dark solution in 5 min, and the mixture was sealed to sonicate at a power of 99W for 20 min at 50 ^{o}C. The obtained suspension was transferred to a 60 mL Teflon-lined stainless-steel autoclave, and maintained at 150 ^{o}C for 24 h. After being cooled to room temperature, the precipitate was collected by centrifuge, washed with ethanol and water for several times and dried at 60 ^{o}C in an oven. The dried sample was then calcined in the tube furnace at 400 ^{o}C for 4 h flowing with argon atmosphere, and the temperature rose from room temperature with an increase rate of 3 ^{o}/min. After grinding, theTiO_2/MLG powder was obtained. The compared TiO_2 sample was prepared in the same method but without the use of multi-layer graphene.

Characterization: The crystallographic structure of the as-prepared materials was studied by X-ray powder diffraction (XRD) using a Bruker D8 diffractometer with monochromatic Cu Kα radiation (λ=1.5406 Å), and the diffraction data was recorded in the 2θ range of 10–80 º. The morphological structures of the anode materials were investigated by a FEI Quanta 200 scanning electron microscopy (SEM) and JEOL 2010F transmission electron microscopy (TEM). The thermogravimetric analysis/differential scanning calorimetry (TGA/DSC) of the samples was carried out on a Diamond TG thermo-analyzer.

Electrochemical tests: The anode was fabricated with the active material, acetylene black, and binder (Polyvinylidene Fluoride, PVDF) in a weight ratio of 8:1:1 by using NMP as solvent and an copper foil as current collector (~ 2.5 mg/cm^2), followed by drying in vacuum at 110 ºC for 24 h. The R2016 coin cell was assembled in an argon-filled glove box using metallic lithium as the cathode and Celgard 2500 membrane as separator. The electrolyte was 1 M $LiPF_6$ dissolved in a mixture of ethylene carbonate (EC), dimethyl carbonate (DMC), diethyl carbonate (DEC) (v/v/v, 1/1/1). Cyclic voltammetry (CV) and galvanostatic charge/discharge cycling tests were carried out in a setting voltage range by using an electrochemical workstation (CHI660C) and a CT2001A LAND battery tester, respectively. Electrochemical impedance spectroscopy (EIS) was studied using a Modulab (Solartron Analytical) with the amplitude of 5 mV in the frequency range from 1 MHz to 10 mHz. All electrochemical tests were carried out at room temperature.

Results and discussion

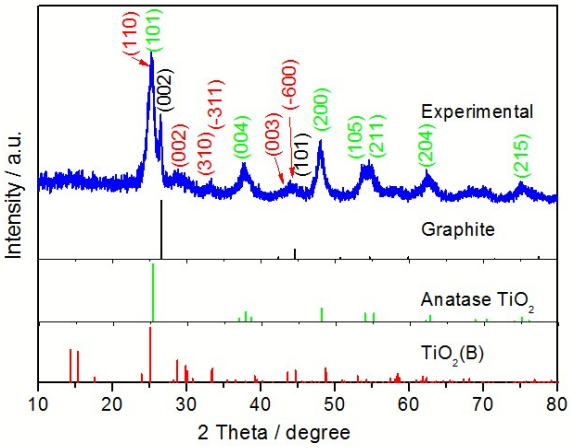

Figure 1. XRD patterns of the as-prepared sample.

The X-ray diffraction (XRD) pattern of the as-prepared composite is shown in Figure 1. The diffraction pattern can be indexed to the three constituent phases of the composite, namely graphite (P63/mmc, JPCD No.65-6212), anatase TiO_2 (I41/amd, JPCD No.65-5714) and TiO_2(B) (C2/m, JPCD No.46-1238). The observed graphite peak is evidence of the incorporation of the multi-layer graphene (MLG) which was used as a reagent during the preparation. The strong (002) diffraction peak at 26.5^{o} illustrates that the MLG structure was maintained throughout the hydrothermal and calcination processes employed in fabrication[43, 44]. TiO_2(B) is formed from the thermal dehydration of layered hydrgen titanate[45, 46], resulting from the low-rate of hydrolysis of TBT in acetic acid. The slow hydrolysis of the TBT precursor with the help of the PVP dispersant is beneficial for the self-assembly of anatase and TiO_2(B). Rietveld refinement of the diffraction pattern using a two-phase analysis model, see **Figure S1**, indicates that the phase content of anatase TiO_2 and TiO_2(B) are 70.7% and 29.3%, respectively.

In order to estimate the amount of MLG in the composite sample, thermal analysis/differential scanning calorimetry (TGA/DSC) was carried out in air with a heating speed of 5 ^{o}C min^{-1} (**Figure S2**). The slight weight loss before 120 ^{o}C is ascribed to the evaporation of adsorbed water molecules. As the complete decomposition temperature of graphene has been generally considered to be around 700 ^{o}C[47-50], the weight loss at this temperature has been assumed to corresond to the content of MLG in the TiO_2/MLG composite, which is estimated to be 5.8 %. In addition, the wide exothermic peaks of TiO_2/MLG reflects the oxidization of the carbon skeleton of

Journal of Materials Chemistry A Accepted Manuscript

This journal is © The Royal Society of Chemistry 20xx

Please do not adjust margins

MLG, which can be affected by the formed C-Ti bond and the distribution of TiO_2 creating localized spots to facilitate the oxidization reaction[51-53]. Besides MLG, the phase transformation of TiO_2 from TiO_2(B) to anatase to rutile in the range of 350 ~ 600 °C causes fluctuations in the exothermic peaks[54, 55].

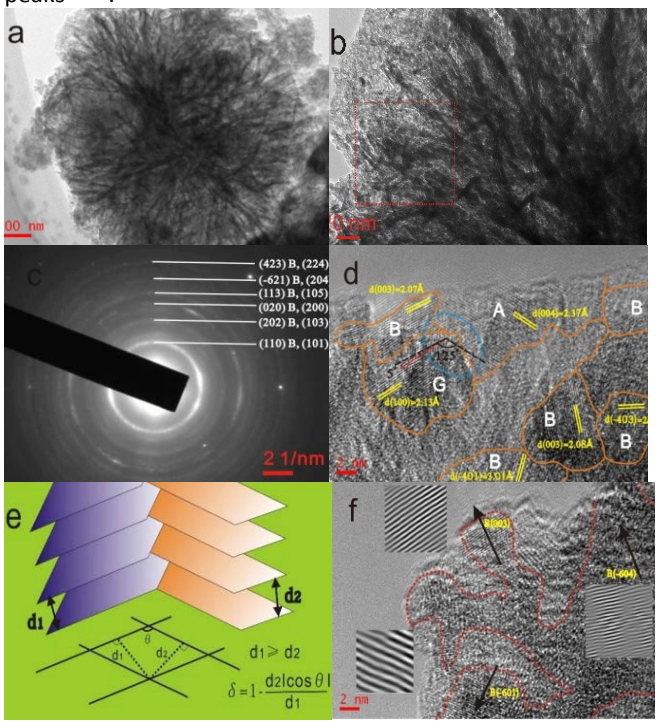

Figure 2. a) TEM image of TiO_2/MLG morphology. b) Magnified TEM image around outer regionof TiO_2/MLG. c) Corresponding SAED pattern of the rectangular area in b). A and B represent anatase TiO_2 and TiO_2(B), respectively. d) HRTEM image with interface lines between phase regions. A, B and G in the image indicate anataseTiO_2, TiO_2(B)and graphene phase, respectively. e) Representation of the interface mismatch rate, δ, between two adjacent phases. f) HRTEM image of the focused limb part with magnified lattice plane by FFT and inverse FFT.

The dandelion-shaped TiO_2/MLG with TiO_2(B) fibrils and anatase TiO_2 pappi was characterized by scanning electron microscopy (SEM) and transmission electron microscopy (TEM). **Figures 2(a) and (b)** show that TiO_2/MLG is composed of connected ultrathin nanowires and nanosheets, with a thickness of several nanometers. The SEM image of TiO_2/MLG is shown in **Figure S3** with the spherical dandelion morphology. The selected area electron diffraction (SAED) pattern shown in **Figure 2c** displays broad diffraction rings that can be assigned to a composite of the two TiO_2 polymorphs, namely anatase TiO_2 and TiO_2(B), and the broad rings assigned to (110), (202), (020), (113), (-621) and (423) planes for TiO_2(B) can also be identified to the (101), (103), (200), (105), (204) and (224) planes of anatase TiO_2[4]. The high resolution transmission electron microscope (HRTEM) image of TiO_2/MLG displayed in **Figure 2d** clearly demonstrates the crystal domains of the three phases in a nano-region, and the boundary structures between anatase TiO_2 and TiO_2(B). Within the triple phase region indicated by an ellipse in **Figure 2(d)**, it is found that the lattice fringes of the (003) plane of TiO_2(B) and the (004) plane of anatase TiO_2 are adjacent with a 125° angular mismatch, and there is a 5° angular mismatch between the (100) plane of graphene and the (003) plane of TiO_2(B) and 120° between the (100) plane of graphene and the (004) plane of anatase TiO_2. As depicted in **Figure 2e**, the interface mismatch rate, δ, between two mismatched phases can be calculated using equation 1 where δ reflects the interface matching intensity or the possibility of interface match[4].

$$\delta = 1 - \frac{d_2|cos\theta|}{d_1} \qquad d_1 \geq d_2 \qquad (1)$$

the schematically presented parameters d_1 and d_2 signify the projected lengths of mismatched planes and equation 1 may be employed when $d_1 \geq d_2$. δ is calculated to be 0.497, 0.032 and 0.539 for the interfaces between the (003) plane of TiO_2(B) and the (004) plane of anatase, the (003) plane of TiO_2(B) and (100) plane of graphene, the (004) plane of anatase and (100) plane of graphene, respectively. More abundant interfacial structrue is present between graphene and anatase in this triphase composite than between anatase and TiO_2(B). By employing Fast Fourier Transform (FFT) and inverse FFT, the magnified lattices of the corresponding darker parts in the HRTEM image displayed in **Figure 2f** are assigned to TiO_2(B), which demonstrates that crystals of this phase form the fibrils whilst the lighter pappi parts are composed of anatase TiO_2 and the complementary analysis is shown in **Figure S4**. In addition, it is clearly observed from the FFT images in **Figure 2f** that the lattice plane of (-604) displays a degree of disorder.

Cyclic Voltammetry (CV) of TiO_2/MLG was implemented in a voltage range of 1-3 V *vs.* Li/Li^+, and the CV curves are shown in **Figure 3a,b**. The first CV cycle, beginning from the open circuit voltage, shows different electrochemical behavior to the subsequent cycles, consistent with conditioning of the anode material during the first round of Li insertion/de-insertion. The second and fourth cycles are consistent in shape illustrating excellent reversibility of the reactions for the as-prepared material[4, 7]. The cathodic peak located at 1.37 V *vs.* Li/Li^+ in the first cycle is found to disappear in the following, which has been explained as the irreversible reactions of some impurities[4]. Compared with the CV peaks of TiO_2(B)[7], the cathodic peak at around 1.4 V in the first cycle results from the open channel saturation of TiO_2(B) by inserted Li^+ ions. In the anodic scan of the second cycle there are three distinct peaks labeled A, B1 and B2 in **Figure 3(a)**. At higher scan rate, **Figure 3(b),** peaks B1 and B2 are less well defined and eventually merge into a single entity labeled B. Analysis of peaks A and B as the scan rate is varied from 0.2 mV s^{-1} to 1.2 mV s^{-1} indicates that the peak current of the former is a linear function of the square root of the scan rate, **Figures 3(c),** whilst the height of the latter is directly proportional to the scan rate, **Figure 3(d)**. The as-prepared TiO_2/MLG includes a mixture of anatase and TiO_2(B) presenting diffusion- and surface-controlled electrochemical reactions at different potentials[3, 4, 7]. The position of peak A, 1.68 V vs. Li/Li^+, and the variation in peak height with scan rate are consistent with lithium insertion into anatase TiO_2[5] . Peak B can be assigned to a pseudocapacitative

Journal of Materials Chemistry A Accepted Manuscript

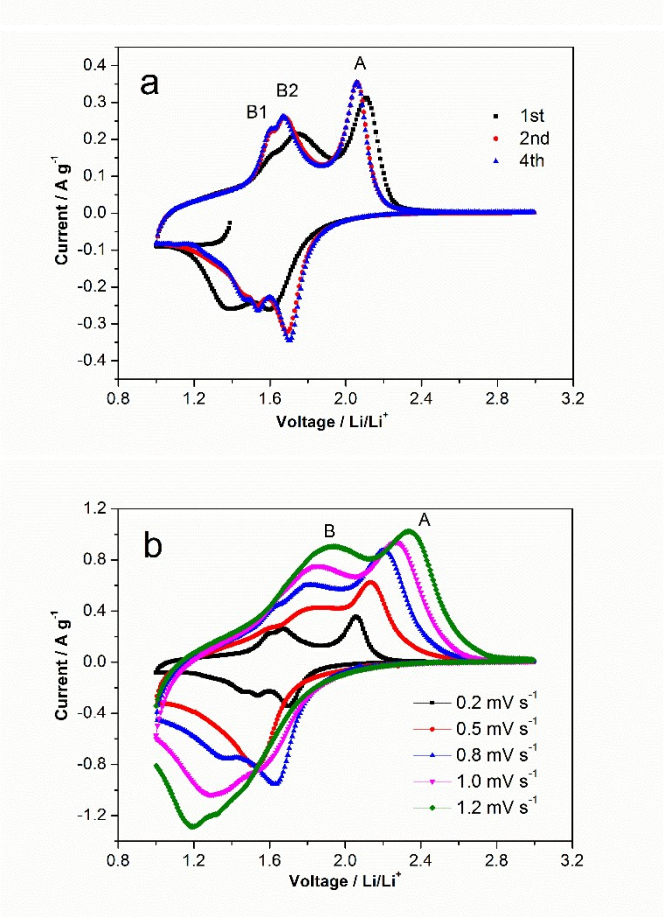

Figure 3. CV curves of TiO_2/MLG. a) The first four cycles at the scan rate of 0.2 mV s^{-1}. b) CV curves at different scan rates from 0.2 to 1.2 mVs^{-1}. Linear relationships of c) the A peak process on the surface of TiO_2(B)[56]. A higher current associated with anatase TiO_2 is in agreement with the composition of the composite.

The galvanostatic charge/discharge profiles in the voltage range of 1 to 3V *vs.* Li/Li^+ of TiO_2/MLG and TiO_2 prepared using the same synthetic method but without MLG are shown in **Figure 4a**. The discharge curves of TiO_2/MLG and TiO_2 can be divided into three regions[36, 57]. The first region (Region1) with a steep decrease in potential is ascribed to the homogeneous Li^+ insertion into bulk TiO_2 until the solid-solution limit of Li^+ ions in TiO_2, such behavior is indicative of a nano-sized titania material[58]. Region 2 is characteristic of the lithiation of anatase. It can be seen that the average voltage plateau of TiO_2/MLG (1.75 V) is 20 mV higher than that of TiO_2 (1.73 V), from which it can be deduced that the boundary structures between TiO_2 and graphene have the potential to lower the electrode polarization resulting from the good electronic and ionic conductivity[44] in the biphase TiO_2 (Li-rich and Li-poor) co-existence plateau[36]. The contributed capacities of 126 and 106 mAh g^{-1} for TiO_2/MLG and TiO_2 in the two regions result from the random insertion of Li^+ into over half the available interstitial octahedral sites of anatase[4, 57]. Region 3, at low potentials, corresponds to the loss of pseudocapacitative charges from the interfaces in the system. The TiO_2/MLG composite anode and the TiO_2 anode have very similar behavior in regions 1 and 2 of the discharge curve indicating that the degree of lithiation of the nanoparticles is independent of the amount of MLG. In region 3 the TiO_2/MLG composite displays a higher specific capacity at all potentials. In the second and third cycles, region3 of TiO_2/MLG composite can be divided into two slopes of different gradient whilst for the TiO_2 anode a single gradient is observed, as shown in **Figure S5**. The columbic efficiency of TiO_2/MLG in the first cycle is 80.4%, slightly higher than the 78.8% observed for the TiO_2 anode.

Figure 4b shows the discharge capacities of TiO_2/MLG at current densities of 0.05, 0.1, 0.2, 0.5, 1, 2, 3 and 5 A g^{-1} are 266, 243, 221, 200, 182, 161, 140 and 115 mAh g^{-1}. For the higher discharge rates of 5.5, 6, 7, 8, and 10 A g^{-1} the capacities of TiO_2/MLG are 84, 69, 48, 43 and 35mAh g^{-1}, as indicated in **Figure 4c**. For comparison, the specific discharge capacities of TiO_2 displayed in **Figure 4d** are 198, 183, 159, 128, 119, 113, 100 and 86 mAh g^{-1} for current densities of 0.05, 0.1, 0.2, 0.5, 0.8, 1, 1.4 and 2 A g^{-1}, respectively. It is found that the specific capacity of TiO_2/MLG at 1 A g^{-1} retains 75% of the value at 0.1 A g^{-1}, while TiO_2 keeps 62%. The cyclic performances of TiO_2/MLG in **Figure 4e** was investigated to evaluate the electrode stability. Only a slight loss of capacity was observed after 100 cycles at a current density of 0.1 A g^{-1}. The corresponding capacity retention of TiO_2/MLG is 99.6% with high coulombic efficiency almost approaching 100%, even for high current rates of 5 and 10 A g^{-1} as illustrated in **Figure S6**. The coulombic efficiencies of the 1200 cycles of TiO_2/MLG are extreme coincident when compared with that of the reference TiO_2 (**Figure S7**), which confirms the high electrode stability of TiO_2/MLG during cycling. With reference to the conclusions from Wu *et. al*[4], the high electrochemical stability of the

Journal of Materials Chemistry A Accepted Manuscript

This journal is © The Royal Society of Chemistry 20xx

Please do not adjust margins

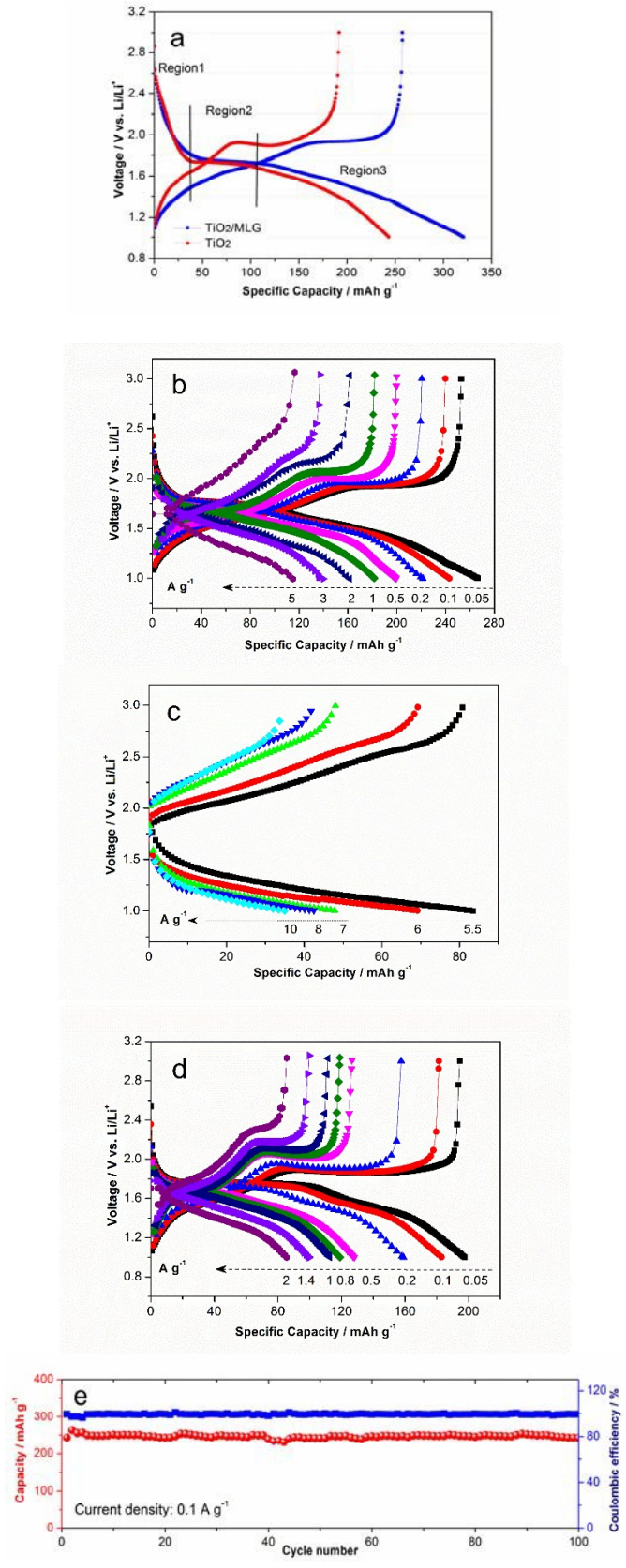

Figure 4. Galvanostatic charge/discharge profiles. a) The first cycle of TiO_2/MLG and TiO_2 at a current density of 0.05 A g^{-1}.b) Rate performances of TiO_2/MLG from 0.05 to 2 A g^{-1} and c) from 5.5 to 10 A g^{-1}. d) Rate performances of TiO_2 from 0.05 to 2 A g^{-1}. e) Cycling performances of TiO_2/MLG at 0.1A g^{-1}.

electrode is attributed to the three-dimensional dandelion-shape microsphere structure which provides short diffusion distance for ion transport, high contact area between the electrolyte and electrode and the boundaries of TiO_2/MLG which are capable of accommodating strain during cycling, leading to high Li^+ diffusion kinetics as well as stable electrochemical reactions.

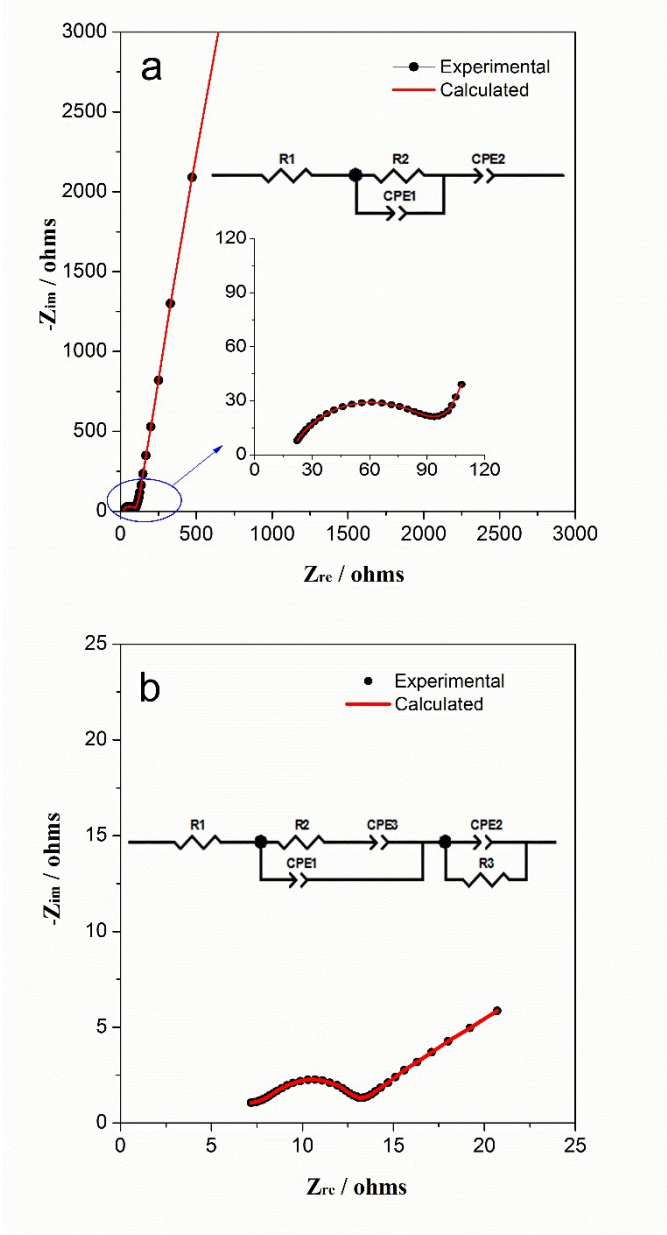

Figure 5. Nyquist plot of TiO_2/MLG cell after a) 0 and b) 1000 cycles with corresponding calculated fitting results. Inset is the corresponding equivalent circuit model.

Electrochemical impedance spectroscopy (EIS) was used to explore the variation of impedance of TiO_2/MLG during electrochemical cycling. **Figures 5(a)** and **(b)** show the Nyquist plots for electrodes cycled 0 and 1000 times with corresponding calculated plots which are obtained from the equivalent circuit model in the insert, respectively. For the

Journal of Materials Chemistry A Accepted Manuscript

components in the equivalent circuit, the values, with errors, that were calculated to yield the best fits to the experimental data are listed in **Table S1** and **S2**. In the equivalent circuit of both, R1 represents the internal resistance of the cell that arises from both the electrode and electrolyte. CPE2 (constant phase element) in **Figure 5(a)** represents the pseudocapacitance that is generated on the complicated surface of internal triphase boundaries[4] plus electrodes. R2 represents the charge transfer and possible ion diffusion, and CPE1 is the capacitor in the bulk associated with Li^+ ions insertion. In **Figure 5(b),** two new components are introduced namely CPE3 and R3. CPE3 is defined as Warburg resistance with the factor, n=0.5 (**Table S2**) and correspondingly, CPE1 becomes pure capacitor with n=1. Warburg resistance results from the solid-state ion diffusion in the electrode channels. The presence of R3 points to the development of a surface resistance during cycling, which can be attibuted to the open interfacial structure in the electrode or SEI film on the electrode surface[4]. According to **Table S1** and **S2**, the resistances, R1 and R2 have decreased but the capacitance of CPE1 and CPE2 have increased after multiple electrochemical cycles when compared with those of the fresh cell. The impedance data indicates that the structural rearrangement of TiO_2/MLG electrode during cycling promotes the boundary storage to be predominant over bulk storage for Li^+ ions. The interfacial structure provides more open channels for ion diffusion with cycling.

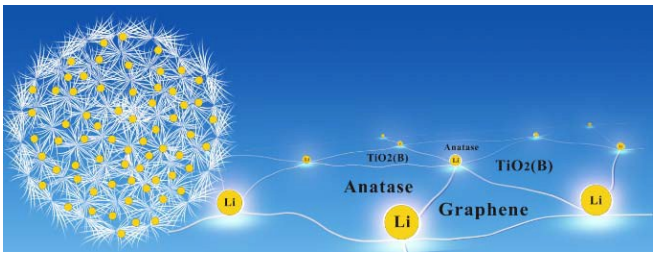

Figure 6. Schematic representation of interfacial storage for Li^+ ions of TiO_2/MLG.

Figure 6 is a schematic representation of the TiO_2/MLG composite. The as-prepared material has an abundance of tri-phase boundaries between anatase TiO_2, TiO_2(B) and graphene. Wang *et al.*[42] have demonstrated that charge storage at the anatase TiO_2-TiO_2(B) junction can enhance Li^+ storage in anode materials. The high specific capacities observed for the biphasic TiO_2 material prepared in the absence of MLG points to a synergistic interfacial effect improving charge storage. The specific capacitance of the dandelion structured TiO_2 is further enhanced when MLG is introduced into the composite. The interfaces within nanosized materials can offer more sites for Li^+ storage[36] and the boundaries between MLG and TiO_2 phases also provide sites for Li storage. The MLG itself with nearly 30 layers will only contribute negligible capacity in the voltage range of 1-3 V *vs.* Li/Li^{+}[59]. There are abundant phase boundaries arising from the polycrystal in TiO_2/MLG dandelion structure, contributing to large extent of lattice mismatch, as well as extra sites for Li^+ ion and electron storage and some disordered planes probably provide more active sites for Li^+ ion storage and transfer[4, 11]. The TiO_2/MLG is able to store charge through both Li^+ insertion and a pseudocapacitative mechanism, as evidenced by the i-V curves obtained when the potential is cycled. We postulate that the improved rate performance of the TiO_2/MLG composite relative to the TiO_2 material results from the fact that the edge-abundant interfaces of graphene can promote the Li^+ ion diffusion and electron transport along the triphase boundaries, as schematically presented in **Figure 6**.

Conclusions

Dandelion-shape TiO_2/MLG composed of TiO_2(B) fibrils and anatase pappi was synthesized as promising anode material for Li storage. Both the material characterization and cyclic voltammetry presenting diffusion- and surface-controlled electrochemical reaction at different potentials, evidenced the anatase/TiO_2(B)heterophase in TiO_2/MLG, and the open channel saturation of TiO_2(B) by inserted Li^+ ions at around 1.4 V was used to explain the irreversible cathodic peak. A mismatch rate, δ, between two adjacent phases with mingled boundaries, was introduced to describe the interplanar mismatch degree. The edge-abundant interfaces of graphene involved in the triphase boundaries were reported to enhance the electrochemical storage properties of TiO_2/MLG and lower the electrode polarization by the improvement of Li^+ diffusion and electron transport. The discharge capacities of TiO_2/MLG at current densities of 0.05, 0.1, 0.2, 0.5, 1, 2, 3 and 5 A g^{-1} are 266, 243, 221, 200, 182, 161, 140 and 115 mAh g^{-1}, and the capacity retention is 99.6% with high coulombic efficiency almost approaching 100% after 100 cycles at the current density of 0.1 A g^{-1}. The resistances of TiO_2/MLG decreased with cycling and more boundaries were opened to enhance ionic and electron conductivity.

Acknowledgements

Financial supports from the Imperial College PhD Scholarship, Engineering and Physical Sciences Research Council (EPSRC, Grant: EP/L015277/1) are greatly appreciated.

Notes and references

1. Y. Tang, Y. Zhang, W. Li, B. Ma and X. Chen, *Chem. Soc. Rev.*, 2015, 5926-5940.
2. B. Kang and G. Ceder, *Nat. Mater.*, 2009, **458**, 190-193.
3. L. Kavan, *J. Solid. State. Electr.*, 2014, **18**, 2297-2306.
4. Q. Wu, J. Xu, X. Yang, F. Lu, S. He, J. Yang, H. J. Fan and M. Wu, *Adv. Energy Mater.*, 2015, **5**, 1401756-1401765.
5. J. Chen, W. Song, H. Hou, Y. Zhang, M. Jing, X. Jia and X. Ji, *Adv. Funct. Mater.*, 2015, **25**, 6793–6801.
6. S. Goriparti, E. Miele, M. Prato, A. Scarpellini, S. Marras, S. Monaco, A. Toma, G. C. Messina, A. Alabastri, F. D. Angelis, L. Manna, C. Capiglia and R. P. Zaccaria, *ACS Appl Mater Interfaces*, 2015, **7**, 25139-25146.
7. B. Laskova, M. Zukalova, A. Zukal, M. Bousa and L. Kavan, *J. Power. Sources*, 2014, **246**, 103-109.
8. H. Ren, R. Yu, J. Wang, Q. Jin, M. Yang, D. Mao, D. Kisailus, H. Zhao and D. Wang, *Nano Lett.*, 2014, **14**, 6679-6684.
9. C. Kim, R. Buonsanti, R. Yaylian, D. J. Milliron and J. Cabana, *Adv. Energy Mater.*, 2013, **3**, 1286-1291.
10. M. Zhao, L. Li, H. Lin, L. Yang and G. Li, *Chem. Commun.*, 2013, **49**, 7046-7048.

Journal of Materials Chemistry A Accepted Manuscript

This journal is © The Royal Society of Chemistry 20xx

Please do not adjust margins

11. Y. Ren, Z. Liu, F. Pourpoint, A. R. Armstrong, C. P. Grey and P. G. Bruce, *Angew. Chem. Int. Ed.*, 2012, **51**, 2164-2167.
12. J. Akimoto, Y. Gotoh, Y. Oosawa, N. Nonose, T. Kumagai, K. Aoki and H. Takei, *J. Solid State Chem.*, 1994, **113**, 27-36.
13. M. Latroche, L. Brohan, R. Marchand and M. Tournoux, *J. Solid State Chem.*, 1989, **81**, 78-82.
14. K. Spektor, D. T. Tran, K. Leinenweber and U. Häussermann, *J. Solid State Chem.*, 2013, **206**, 209-216.
15. H. SATO, S. ENDO, M. SUGIYAMA, T. KIKEGAWA, O. SHIMOMURA and K. KUSABA, *Science*, 1991, **251**, 786-788.
16. Y. Al-Khatatbeh, K. K. M. Lee and B. Kiefer, *Phys. Rev. B.*, 2009, **79**.
17. M. Mattesini, J. S. de Almeida, L. Dubrovinsky, N. Dubrovinskaia, B. Johansson and R. Ahuja, *Phys. Rev. B.*, 2004, **70**.
18. N. A. Dubrovinskaia, L. S. Dubrovinsky, R. Ahuja, V. B. Prokopenko, V. Dmitriev, H. P. Weber, J. M. Osorio-Guillen and B. Johansson, *Phys. Rev. Lett.*, 2001, **87**, 275501.
19. L. S. Dubrovinsky, N. A. Dubrovinskaia, V. Swamy, J. Muscat, N. M. Harrison, R. Ahuja, B. Holm and B. Johansson, *Nature*, 2001, **410**, 653-654.
20. D. O. Scanlon, C. W. Dunnill, J. Buckeridge, S. A. Shevlin, A. J. Logsdail, S. M. Woodley, C. R. A. Catlow, M. J. Powell, R. G. Palgrave, I. P. Parkin, G. W. Watson, T. W. Keal, P. Sherwood, A. Walsh and A. A. Sokol, *Nat. Mater.*, 2013, **12**, 798-801.
21. D. D'Elia, École Nationale Supérieure des Mines de Paris, 2011.
22. S. Moitzheim, C. S. Nimisha, S. Deng, D. J. Cott, C. Detavernier and P. M. Vereecken, *Nanotechnology*, 2014, **25**, 504008.
23. T. Zhou, Y. Zheng, H. Gao, S. Min, S. Li, H. K. Liu and Z. Guo, *Adv. Sci.*, 2015, **2**, 1500027.
24. S. Li, M. Ling, J. Qiu, J. Han and S. Zhang, *J. Mater. Chem. A*, 2015, **3**, 9700-9706.
25. X. Yan, Y. Li, M. Li, Y. Jin, F. Du, G. Chen and Y. Wei, *J. Mater. Chem. A*, 2015, **3**, 4180-4187.
26. K. Siuzdak, R. Bogdanowicz, M. Sawczak and M. Sobaszek, *Nanoscale*, 2015, **7**, 551-558.
27. X. Yang, Y. Yang, H. Hou, Y. Zhang, L. Fang, J. Chen and X. Ji, *The Journal of Physical Chemistry C*, 2015, **119**, 3923-3930.
28. Z. Hong, M. Wei, T. Lan, L. Jiang and G. Cao, *Energ. Environ. Sci.*, 2012, **5**, 5408-5413.
29. G. Li, Z. Lian, X. Li, Y. Xu, W. Wang, D. Zhang, F. Tian and H. Li, *J. Mater. Chem. A*, 2015, **3**, 3748-3756.
30. H. Tian, F. Xin, X. Tan and W. Han, *J. Mater. Chem. A*, 2014, **2**, 10599-10606.
31. S. Wei, R. Wu, J. Jian, F. Chen and Y. Sun, *Dalton Trans.*, 2015, **44**, 1534-1538.
32. W. Jiao, N. Li, L. Wang, L. Wen, F. Li, G. Liu and H.-M. Cheng, *Chem. Commun.*, 2013, **49**, 3461-3463.
33. W. Zhang, Y. Gong, N. P. Mellott, D. Liu and J. Li, *J. Power. Sources*, 2015, **276**, 39-45.
34. Z. Ali, S. N. Cha, J. I. Sohn, I. Shakir, C. Yan, J. M. Kim and D. J. Kang, *J. Mater. Chem.*, 2012, **22**, 17625-17629.
35. M. Lübke, I. Johnson, N. M. Makwana, D. Brett, P. Shearing, Z. Liu and J. A. Darr, *J. Power. Sources*, 2015, **294**, 94-102.
36. J.-Y. Shin, D. Samuelis and J. Maier, *Adv. Funct. Mater.*, 2011, **21**, 3464-3472.
37. J. Maier, *Nat. Mater.*, 2005, **4**, 805-815.
38. J. Jamnik and J. Maier, *Phys. Chem. Chem. Phys.*, 2003, **5**, 5215-5220.
39. Y. F. Zhukovskii, P. Balaya, E. A. Kotomin and J. Maier, *Phys Rev Lett*, 2006, **96**, 058302.
40. D. Yang, H. Liu, Z. Zheng, Y. Yuan, J.-c. Zhao, E. R. Waclawik, X. Ke and H. Zhu, *Journal of the American Chemical Society*, 2009, **131**, 17885-17893.
41. N. Fu, Y. Wu, Z. Jin and G. Lu, *Langmuir*, 2010, **26**, 447-455.
42. R. Wang, X. Xue, W. Lu, H. Liu, C. Lai, K. Xi, Y. Che, J. Liu, S. Guo and D. Yang, *Nanoscale*, 2015, **7**, 12833-12838.
43. W. Song, X. Cao, Z. Wu, J. Chen, Y. Zhu, H. Hou, Q. Lan and X. Ji, *Langmuir*, 2014, **30**, 12438-12446.
44. W. Song, X. Ji, Z. Wu, Y. Zhu, Y. Yang, J. Chen, M. Jing, F. Li and C. E. Banks, *J. Mater. Chem. A*, 2014, **2**, 5358-5362.
45. G. Armstrong, A. R. Armstrong, J. Canales and P. G. Bruce, *Chem. Commun.*, 2005, 2454-2456.
46. T. P. Feist and P. K. Davies, *J. Solid State Chem.*, 1992, **101**, 275-295.
47. N. Li, G. Liu, C. Zhen, F. Li, L. Zhang and H.-M. Cheng, *Adv. Funct. Mater.*, 2011, **21**, 1717-1722.
48. X. Huang, K. Wang, K. Jia and X. Liu, *Polym Advan Technol*, 2015, **26**, 1267-1274.
49. H. Sun, S. Liu, S. Liu and S. Wang, *Appl. Catal. B: Environ.*, 2014, **146**, 162-168.
50. J. S. Chen, Z. Wang, X. C. Dong, P. Chen and X. W. Lou, *Nanoscale*, 2011, **3**, 2158-2161.
51. L. Wang, L. Shen, Y. Li, L. Zhu, J. Shen and L. Wang, *Int. J. Photoenergy.*, 2013, **2013**, 1-7.
52. Q. Huang, S. Tian, D. Zeng, X. Wang, W. Song, Y. Li, W. Xiao and C. Xie, *ACS Catal.*, 2013, **3**, 1477-1485.
53. Y. Gao, X. Pu, D. Zhang, G. Ding, X. Shao and J. Ma, *Carbon*, 2012, **50**, 4093-4101.
54. M. Hu, M. Fang, C. Tang, T. Yang, Z. Huang, Y. Liu, X. Wu and X. Min, *Nanoscale Res. Lett.*, 2013, **8**, 548-548.
55. D. A. H. Hanaor and C. C. Sorrell, *J. Mater. Sci.*, 2010, **46**, 855-874.
56. M. Zukalová, M. Kalbáč, L. Kavan, I. Exnar and M. Graetzel, *Chem. Mater.*, 2005, **17**, 1248-1255.
57. Y.-G. Guo, Y.-S. Hu and J. Maier, *Chem. Commun.*, 2006, 2783.
58. Y. S. Hu, L. Kienle, Y. G. Guo and J. Maier, *Adv. Mater.*, 2006, **18**, 1421-1426.
59. E. Yoo, J. Kim, E. Hosono, H.-s. Zhou, T. Kudo and I. Honma, *Nano Lett.*, 2008, **8**, 2277-2282.

Journal of Materials Chemistry A Accepted Manuscript